

# The Sodium (Iso)Cyanurates $\text{Na}_x[\text{H}_{3-x}\text{C}_3\text{N}_3\text{O}_3]\cdot y\text{H}_2\text{O}$ ( $x = 1-3$ , $y = 0, 1$ ): A Key-Series for Understanding the Crystal Chemistry of Metal (Iso)Cyanurates

Peter Gross<sup>[a]</sup> and Henning A. Höpfe<sup>\*[a]</sup>

*Dedicated to Professor Thomas Fässler on the Occasion of his 60th Birthday*

**Abstract.** The (iso)cyanurates  $\text{Na}[\text{H}_2\text{C}_3\text{N}_3\text{O}_3]\cdot\text{H}_2\text{O}$ ,  $\text{Na}_2[\text{HC}_3\text{N}_3\text{O}_3]\cdot\text{H}_2\text{O}$ ,  $\text{Na}_2[\text{HC}_3\text{N}_3\text{O}_3]$ , and  $\text{Na}_3[\text{C}_3\text{N}_3\text{O}_3]$  were synthesized phase pure from  $\text{Na}_2\text{CO}_3\cdot 10\text{H}_2\text{O}$ ,  $\text{NaOH}$ , and cyanuric acid, respectively, in aqueous solution by carefully adjusting the crystallization conditions. The crystal structures of all compounds were determined by single-crystal X-ray diffraction  $\{\text{Na}_2[\text{HC}_3\text{N}_3\text{O}_3]\cdot\text{H}_2\text{O}$ :  $P\bar{1}$ ,  $a = 3.51660(10)$  Å,  $b = 7.8300(3)$  Å,  $c = 11.3966(4)$  Å,  $\alpha = 86.4400(10)^\circ$ ,  $\beta = 85.5350(10)^\circ$ ,  $\gamma = 85.0720(10)^\circ$ ,  $Z = 2$ ,  $R_1 = 0.030$ ,  $wR_2 = 0.078$ ;  $\text{Na}_2[\text{HC}_3\text{N}_3\text{O}_3]$ :  $Pnma$ ,  $a = 6.3409(6)$  Å,  $b = 12.2382(13)$  Å,  $c = 6.5919(7)$  Å,  $Z = 4$ ,  $R_1 = 0.045$ ,  $wR_2 = 0.079$ ;

$\text{Na}_3[\text{C}_3\text{N}_3\text{O}_3]$ :  $R\bar{3}c$ ,  $a = 11.7459(3)$  Å,  $c = 6.5286(3)$  Å,  $Z = 3$ ,  $R_1 = 0.039$ ,  $wR_2 = 0.066$ }. The structures show ribbons ( $\text{Na}[\text{H}_2\text{C}_3\text{N}_3\text{O}_3]\cdot\text{H}_2\text{O}$ ), dimers ( $\text{Na}_2[\text{HC}_3\text{N}_3\text{O}_3]\cdot\text{H}_2\text{O}$ ), chains ( $\text{Na}_2[\text{HC}_3\text{N}_3\text{O}_3]$ ), or columns ( $\text{Na}_3[\text{C}_3\text{N}_3\text{O}_3]$ ) of hydrogen-bonded and parallel stacked (iso)cyanurate anions. These motifs are shown to be characteristic for certain degrees of protonation and hydration, and all (iso)cyanurate crystal structures found so far were classified accordingly. X-ray powder patterns, thermogravimetry curves, IR and UV/Vis spectra were measured for all compounds.

## Introduction

Though cyanuric acid is a high volume industrial chemical (worldwide production over 100 000 t/a<sup>[1]</sup>) and pivotal to a whole spectrum of industries,<sup>[2-4]</sup> even its simple metal salts are surprisingly sparsely explored by structure elucidation techniques. A few years ago, only the crystal structures of two alkaline earth,<sup>[5,6]</sup> a few alkali,<sup>[7-9]</sup> and some 3d-transition metal<sup>[10-17]</sup> isocyanurates were reported, all except one<sup>[8]</sup> exclusively containing monobasic isocyanurate anions and crystallized from aqueous solution. Scientific interest in the topic has considerably risen since the discovery of the remarkable non-linear optical properties of  $\text{Ca}_3[\text{C}_3\text{N}_3\text{O}_3]_2$ ,<sup>[18]</sup> focussing mainly on tribasic salts of divalent metal ions obtained via solid state methods.<sup>[19-28]</sup> Recently, we accomplished to fuse these two branches of metal (iso)cyanurate chemistry within a broad structural and thermal study of alkali and alkaline earth isocyanurates by successfully preparing the full range of mono-, di- and tribasic (iso)cyanurate salts directly from aqueous solution.<sup>[29]</sup>

In that preceding study we encountered a variety of structural motifs, ranging from the well known isocyanurate ribbon

uniformly found for monobasic salts<sup>[16]</sup> to isocyanurate dimers and chains for dibasic salts as well as columns for tribasic salts, the latter of which are also known from various compounds synthesized via solid state approaches.<sup>[18-28]</sup> In order to shed light on the relationship between degree of deprotonation, crystal water content and formed structural motif, we looked for a series of salts which does not incorporate other chemical species except metal cation, (iso)cyanurate anion and water, as it is well known that the structural pattern is mainly governed by intermolecular hydrogen bonds,<sup>[30,31]</sup> and found the  $\text{Na}_x[\text{H}_{3-x}\text{C}_3\text{N}_3\text{O}_3]\cdot y\text{H}_2\text{O}$  series. Within this series, only  $\text{Na}[\text{H}_2\text{C}_3\text{N}_3\text{O}_3]\cdot\text{H}_2\text{O}$  had been structurally characterized so far, showing the familiar ribbon motif.<sup>[9]</sup>

Besides questions of structural chemistry, a thorough characterization of sodium isocyanurates might also be of considerable interest to environmental chemists,<sup>[2,32]</sup> biochemists,<sup>[33,34]</sup> and toxicologists,<sup>[35,36]</sup> as sodium isocyanurates are not only the most common precursors<sup>[1]</sup> to, but also the main degradation products<sup>[37]</sup> of chlorinated isocyanuric acid derivatives used as swimming pool disinfectants, as well as likely degradation products of atrazine and related s-triazine herbicides. The first description of a member of the  $\text{Na}_x[\text{H}_{3-x}\text{C}_3\text{N}_3\text{O}_3]\cdot y\text{H}_2\text{O}$  series is given by *Hofmann*<sup>[38]</sup> with  $\text{Na}_3[\text{C}_3\text{N}_3\text{O}_3]$ , including synthesis instructions for phase pure products, common impurities, description of crystal morphologies and chemical analysis. Later, there have been some toxicological studies<sup>[35-37,39-41]</sup> of presumably monosodium isocyanurate (no analytical data regarding the probed substance were given) as well as studies regarding infrared spectroscopy and thermal behavior of  $\text{Na}[\text{H}_2\text{C}_3\text{N}_3\text{O}_3]$ , which are summarized within an extensive review by *Seifer*.<sup>[42]</sup>

\* Prof. Dr. H. A. Höpfe  
E-Mail: henning@ak-hoeppe.de

[a] Institut für Chemie  
Universität Augsburg  
Universitätsstr. 1

86159 Augsburg, Germany

Supporting information for this article is available on the WWW under <http://dx.doi.org/10.1002/zaac.201800438> or from the author.

## Results

### $\text{Na}[\text{H}_2\text{C}_3\text{N}_3\text{O}_3]\cdot\text{H}_2\text{O}$

We redetermined the crystal structure of  $\text{Na}[\text{H}_2\text{C}_3\text{N}_3\text{O}_3]\cdot\text{H}_2\text{O}$  and confirm the initial report by Zhu et al.<sup>[9]</sup> and would therefore like to refer the reader to their publication for a general discussion of the structure. According to the X-ray powder diffraction pattern (Figure S1, Supporting Information), we were able to synthesize phase pure samples of  $\text{Na}[\text{H}_2\text{C}_3\text{N}_3\text{O}_3]\cdot\text{H}_2\text{O}$ . The FT-IR spectrum is shown in Figure 1, the frequencies of all peaks are tabulated in Table S1 (Supporting Information) and assigned to vibrational modes to the best of the authors' knowledge, as well as compared to frequencies of other monobasic isocyanurates and cyanuric acid. The frequencies of all observed bands correspond well with the expected frequencies of the assumed chemical species.<sup>[42,43]</sup> The UV/Vis spectrum (Figure S2, Supporting Information) shows a distinct bandgap absorption edge at about 245 nm, similar to other alkali (iso)cyanurates.<sup>[29]</sup>

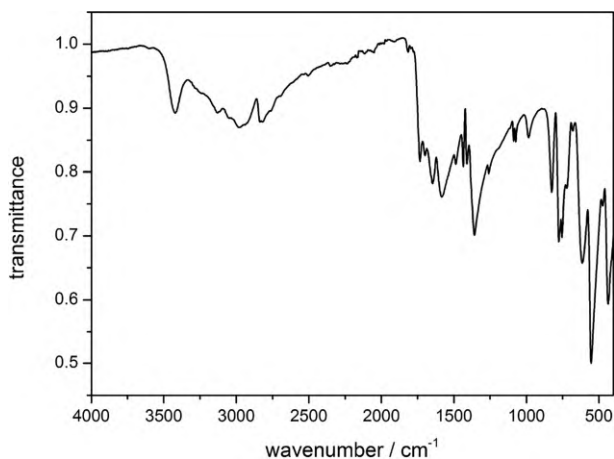


Figure 1. FT-IR spectrum of  $\text{Na}[\text{H}_2\text{C}_3\text{N}_3\text{O}_3]\cdot\text{H}_2\text{O}$ .

Subsequently we studied the thermal decomposition behavior by thermogravimetry (Figure 2). Three major steps of mass loss can be seen. The first, sharp and well defined step ranges from 170 °C to 195 °C and the mass loss accounts to 10.7%.

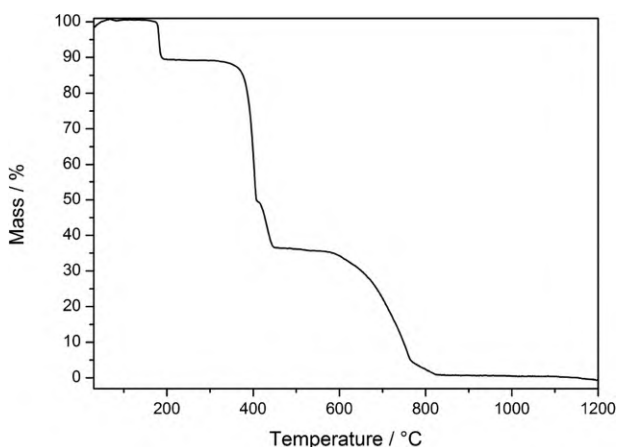


Figure 2. TG curve of  $\text{Na}[\text{H}_2\text{C}_3\text{N}_3\text{O}_3]\cdot\text{H}_2\text{O}$ .

The second step consists of two substeps: one major step starting from about 340 °C with a mass loss of 39.6% and one shoulder starting at about 410 °C and finished at 450 °C with a mass loss of 13.2%. The third step consists of three substeps, of which the first two are strongly overlapping and can only be differentiated by a change of the slope. The first step ranges from about 570 °C to about 665 °C with a mass loss of 7.6%, the second from about 665 °C to about 765 °C with a mass loss of 23.3%, and the third from about 765 °C to about 830 °C 4.3%. The overall mass loss accounts to 99.4%.

### $\text{Na}_2[\text{HC}_3\text{N}_3\text{O}_3]\cdot\text{H}_2\text{O}$

$\text{Na}_2[\text{HC}_3\text{N}_3\text{O}_3]\cdot\text{H}_2\text{O}$  crystallizes in its own structure type in space group  $P\bar{1}$  (no. 2), its unit cell is depicted in Figure 3. The crystal structure exhibits planar dibasic isocyanurate anions  $[\text{HC}_3\text{N}_3\text{O}_3]^{2-}$  (Figure 4a) with typical bond lengths (1.36 Å for C–N and 1.26 Å for C–O) and angles. These anions form dimers via two strong hydrogen bonds between the protonated nitrogen atoms and the carbonyl oxygen atom of two neighboring anions (Figure 4b). The dimers are aligned parallel to  $(\bar{3}1\bar{2})$  and stacked parallel offset along  $(100)$ , thus forming columns with rhomboidal cross section (Figure 4c). The columns are arranged in a simple tetragonal rod packing (Figure 4d).

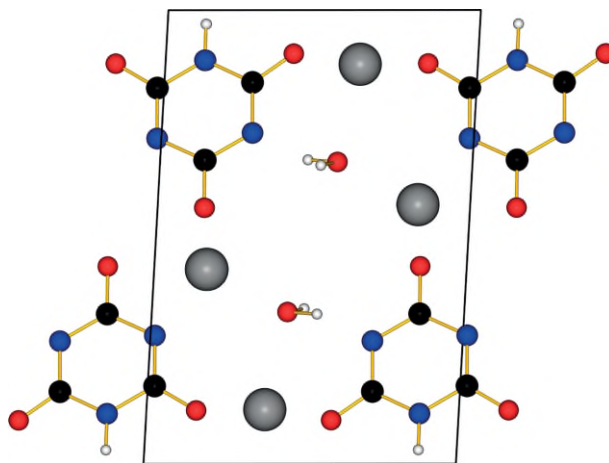
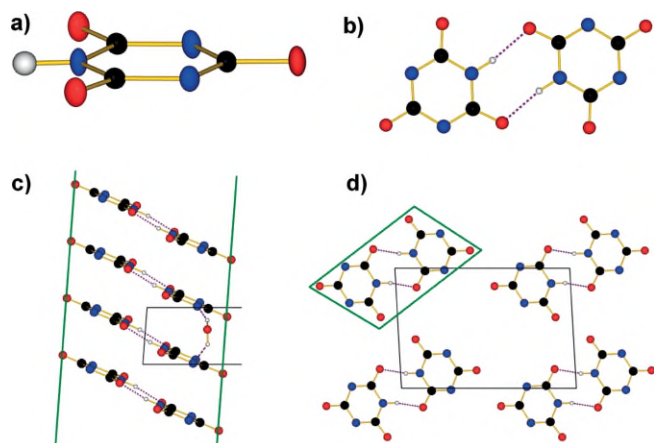


Figure 3. The unit cell of  $\text{Na}_2[\text{HC}_3\text{N}_3\text{O}_3]\cdot\text{H}_2\text{O}$  viewed along  $[100]$ . (Na: grey spheres, C: black spheres, N: blue spheres, O: red spheres and H: white spheres, covalent bonds: yellow sticks).

The  $\text{H}_2\text{O}$  molecules and the  $\text{Na}^+$  cations are located in the voids between these columns, the latter forming layers. The  $\text{H}_2\text{O}$  molecules further connect  $[\text{HC}_3\text{N}_3\text{O}_3]^{2-}$  dimers from neighboring layers of the same column by forming hydrogen bonds towards the deprotonated N atoms of two stacked  $[\text{HC}_3\text{N}_3\text{O}_3]^{2-}$  anions (Figure 4c). Na atoms are found on two different crystallographic sites, Na1 and Na2, as shown in Figure 5. The coordination polyhedron of Na1 can be described as a distorted octahedron (CN = 6), which is spanned by one water molecule and five carbonyl oxygen atoms. The interatomic distances between Na1 and the surrounding atoms correspond on average (2.46 Å) sufficiently well with the sum of the ionic radii (2.40 Å). The coordination polyhedron of



**Figure 4.** Ball-and-stick model of the  $[\text{HC}_3\text{N}_3\text{O}_3]_2^-$  anion of  $\text{Na}_2[\text{HC}_3\text{N}_3\text{O}_3]\cdot\text{H}_2\text{O}$  (hydrogen bonds: broken violet lines); (a) atoms shown as thermal anisotropic ellipsoids (50%); (b) isocyanurate dimer depicted from top; (c) column resulting from stacked isocyanurate dimers; (d) rod packing of columns (solid green lines indicate column faces).

$\text{Na}_2$  can be either described as a distorted square pyramid, spanned by one water molecule, three carbonyl oxygen atoms and one deprotonated nitrogen atom, and capped on the square face by one additional deprotonated nitrogen atom (CN = 5+1) at a considerably longer distance (3.11 Å), or as heavily distorted octahedron (CN = 6). The agreement between the averaged interatomic distances between  $\text{Na}_2$  and the surrounding atoms (2.50 Å for CN = 6 and 2.38 Å for CN = 5) and the sum of the respective ionic radii (2.43 Å for CN = 6 and 2.38 Å for CN = 5) rather indicates that coordination number 5+1 is the more adequate description. Nevertheless, both will be considered as octahedra for exploring the cation substructure. Both types of octahedra are condensed via four common edges to neighboring octahedra belonging to the same type and via one corner to an octahedron belonging to the respective other type, thus forming a layer consisting alternately of  $\text{TiO}_2/\text{Anatase}$ -type slabs and  $\text{ReO}_3$ -type slabs (Figure 6).

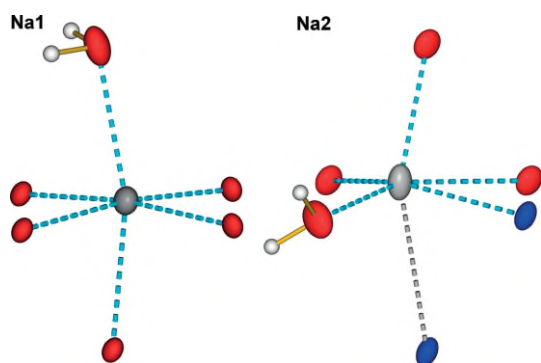


**Figure 5.** Coordination environment of the Na atoms in  $\text{Na}_2[\text{HC}_3\text{N}_3\text{O}_3]\cdot\text{H}_2\text{O}$ , with atoms shown as thermal anisotropic ellipsoids (50%) and interatomic distances represented by broken, light blue (typical distances) and broken, grey (unusually long distances) lines.

According to the X-ray powder diffraction pattern (Figure S3, Supporting Information), we were able to synthesize phase

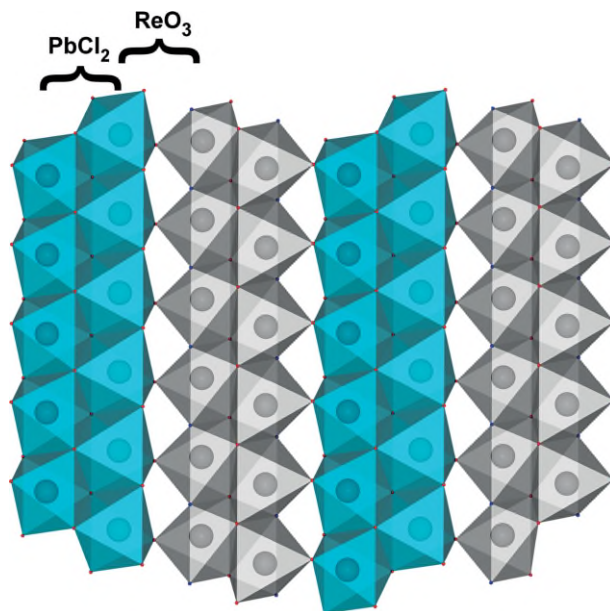


**Figure 6.** Polyhedral representation of cation environments in  $\text{Na}_2[\text{HC}_3\text{N}_3\text{O}_3]\cdot\text{H}_2\text{O}$  as light blue octahedra around  $\text{Na}_1$  and grey octahedra around  $\text{Na}_2$ . The condensation pattern within the layer resembles alternate slabs of Anatase type and  $\text{ReO}_3$  type.

pure samples of  $\text{Na}_2[\text{HC}_3\text{N}_3\text{O}_3]\cdot\text{H}_2\text{O}$ . The FT-IR spectrum is shown in Figure 7, the frequencies of all peaks are tabulated in Table S2 (Supporting Information) and assigned to vibrational modes to the best of the authors' knowledge, as well as compared to frequencies of other dibasic isocyanurates and cyanuric acid. The frequencies of all observed bands correspond well with the expected frequencies of the assumed chemical species.<sup>[42,43]</sup> The UV/Vis spectrum (Figure S4, Supporting Information) shows a distinct bandgap absorption edge at about 245 nm, similar to other alkali (iso)cyanurates.<sup>[29]</sup>

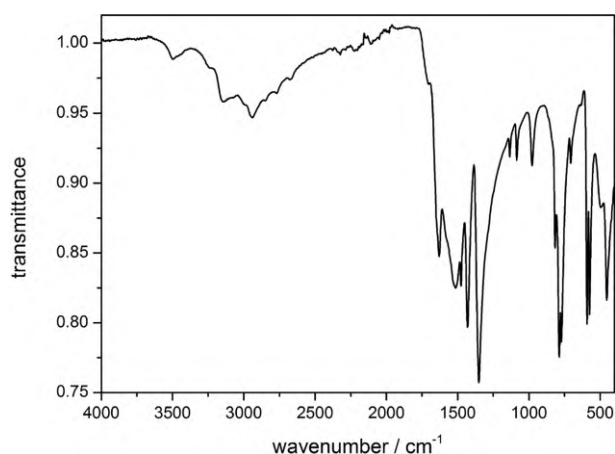


**Figure 7.** FT-IR spectrum of  $\text{Na}_2[\text{HC}_3\text{N}_3\text{O}_3]\cdot\text{H}_2\text{O}$ .

The thermal decomposition behavior was studied via thermogravimetry (Figure 8). Four major steps of mass loss can be seen. The first step ranges from about 100 °C to about 130 °C with a mass loss of 9.6%. The second step ranges from about 300 °C to about 450 °C with a mass loss of 23.7%. The third

step ranges from about 475 °C to about 810 °C with a mass loss of 15.1%. The fourth step ranges from about 810 °C to about 1000 °C with a mass loss of 6.4%.

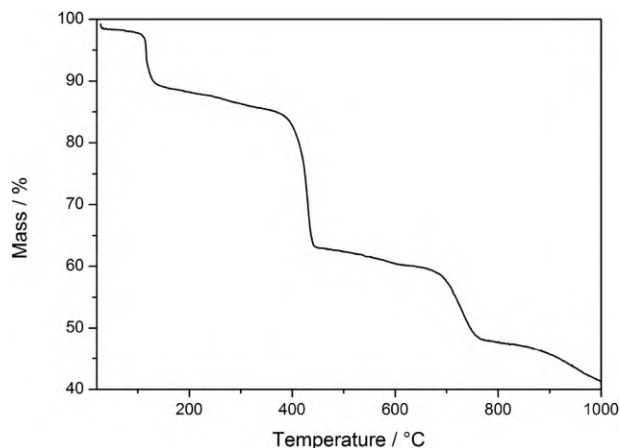


**Figure 8.** TG curve of  $\text{Na}[\text{HC}_3\text{N}_3\text{O}_3]\cdot\text{H}_2\text{O}$ .

### $\text{Na}_2[\text{HC}_3\text{N}_3\text{O}_3]$

$\text{Na}_2[\text{HC}_3\text{N}_3\text{O}_3]$  crystallizes in its own structure type in space group *Pnma* (no. 62), its unit cell is depicted in Figure 9. The crystal structure exhibits planar dibasic isocyanurate anions  $[\text{HC}_3\text{N}_3\text{O}_3]^{2-}$  aligned parallel to (1 0 0) with typical bond lengths (1.35 Å for C–N and 1.26 Å for C–O) and angles (Figure 10a). These anions form slightly undulated chains via hydrogen bonds between a protonated nitrogen atom and a carbonyl oxygen atom of a neighboring anion (Figure 10b). The chains are stacked antiparallel offset along (1 0 0), thus forming layers (Figure 10c).

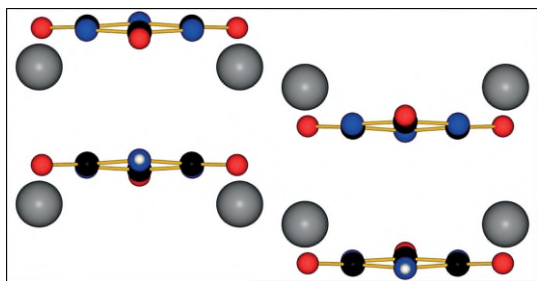


**Figure 9.** The unit cell of  $\text{Na}_2[\text{HC}_3\text{N}_3\text{O}_3]$  viewed along [100]. (Na: grey spheres, C: black spheres, N: blue spheres, O: red spheres and H: white spheres, covalent bonds: yellow sticks).

The  $\text{Na}^+$  cations are located between these anion layers on a single crystallographic site, forming a heavily distorted, puckered close-packed layer. The coordination polyhedron around Na can be described as a distorted trigonal prism (CN = 6), which is spanned by four carbonyl oxygen atoms and two deprotonated nitrogen atoms (Figure 11a). These prisms are condensed via three common edges and one common corner within the close-packed layers and via two common corners between the close-packed layers (Figure 12). The interatomic distances between Na and the surrounding atoms

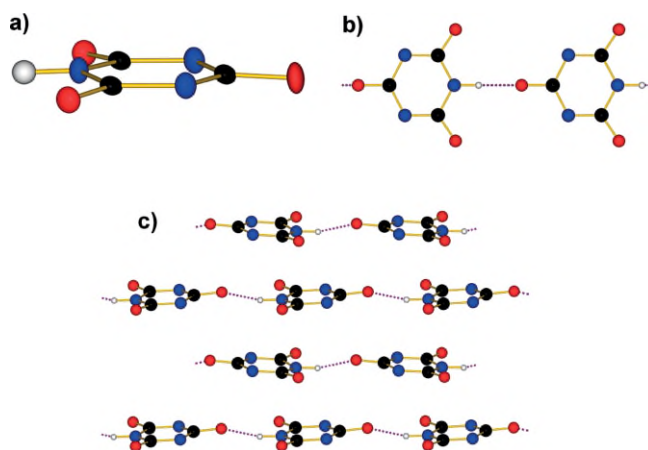


**Figure 10.** Ball-and-stick model of the  $[\text{HC}_3\text{N}_3\text{O}_3]^{2-}$  anion of  $\text{Na}_2[\text{HC}_3\text{N}_3\text{O}_3]$  (hydrogen bonds: broken violet lines); (a) atoms shown as thermal anisotropic ellipsoids (50%); (b) isocyanurate chain depicted from top; (c) layers resulting from stacked isocyanurate chains.

correspond on average (2.50 Å) reasonably well with the sum of the ionic radii (2.43 Å).

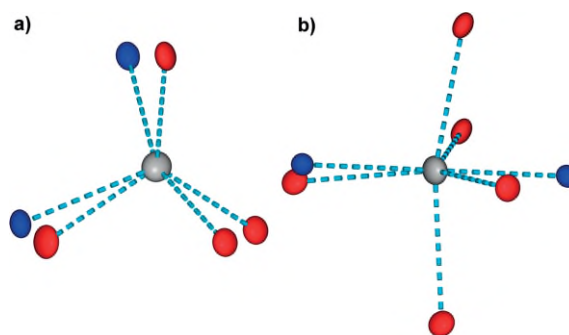


**Figure 11.** Coordination environment of the Na atom in (a)  $\text{Na}_2[\text{HC}_3\text{N}_3\text{O}_3]$  and (b)  $\text{Na}_3[\text{C}_3\text{N}_3\text{O}_3]$ , with atoms shown as thermal anisotropic ellipsoids (50%) and interatomic distances represented by broken, light blue lines.

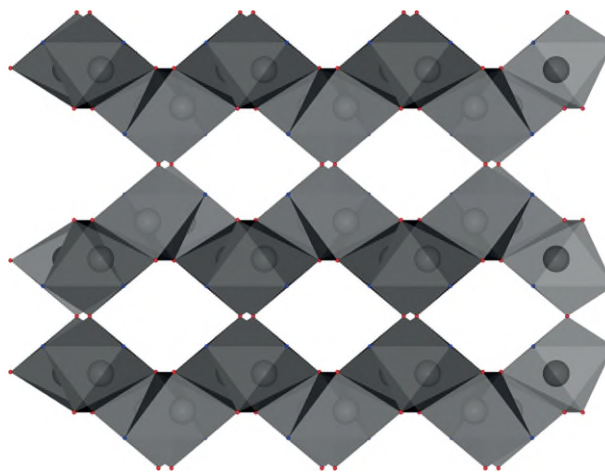


**Figure 12.** Polyhedral representation of the cation environment as grey trigonal prisms of  $\text{Na}_2[\text{HC}_3\text{N}_3\text{O}_3]$ .

According to the X-ray powder diffraction pattern (Figure S5, Supporting Information), we were able to synthesize phase

pure samples of  $\text{Na}_2[\text{HC}_3\text{N}_3\text{O}_3]$ . The FT-IR spectrum is shown in Figure 13, the frequencies of all peaks are tabulated in Table S2 (Supporting Information) and assigned to vibrational modes to the best of the authors' knowledge, as well as compared to frequencies of other dibasic isocyanurates and cyanuric acid. The frequencies of all observed bands correspond well with the expected frequencies of the assumed chemical species.<sup>[42,43]</sup> The UV/Vis spectrum (Figure S6, Supporting Information) shows a distinct bandgap absorption edge at about 245 nm, similar to other alkali (iso)cyanurates.<sup>[29]</sup>

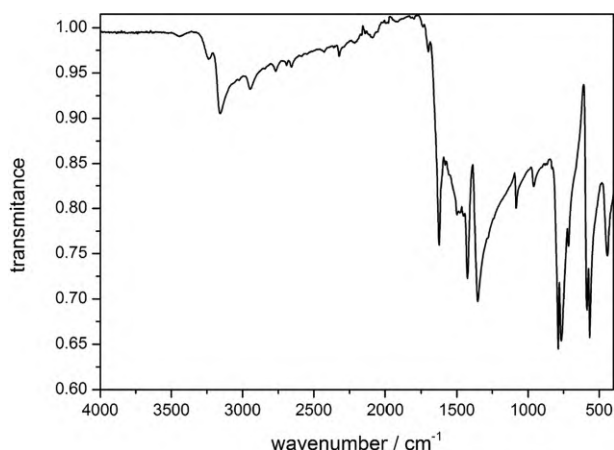


**Figure 13.** FT-IR spectrum of  $\text{Na}_2[\text{HC}_3\text{N}_3\text{O}_3]$ .

The thermal decomposition behavior was studied by thermogravimetry (Figure 14). Two major steps of mass loss can be seen. The first step ranges from about 340 °C to about 450 °C with a mass loss of 23.7%. The second step consists of two substeps, which are strongly overlapping and can only be differentiated by a distinct change of the slope. The first substep ranges from about 575 °C to about 845 °C with a mass loss of 31.0%, the second substep from about 845 °C to about 920 °C with a mass loss of 33.2%.

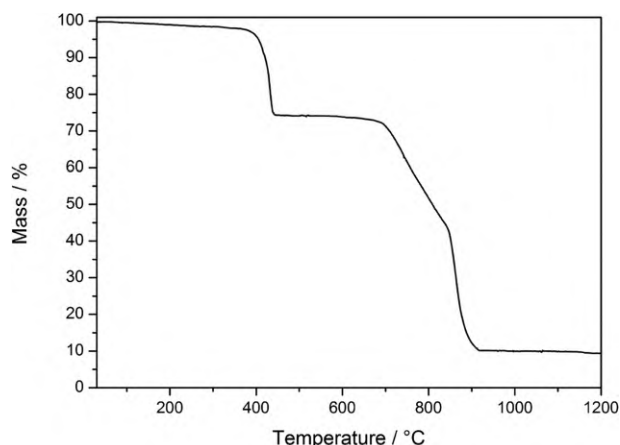


**Figure 14.** TG curve of  $\text{Na}[\text{H}_2\text{C}_3\text{N}_3\text{O}_3]$ .

### $\text{Na}_3[\text{C}_3\text{N}_3\text{O}_3]$

$\text{Na}_3[\text{C}_3\text{N}_3\text{O}_3]$  crystallizes in its own structure type in space group  $R\bar{3}c$  (no. 167), its unit cell is depicted in Figure 15. The

crystal structure exhibits tribasic cyanurate anions  $[\text{C}_3\text{N}_3\text{O}_3]^{3-}$  (Figure 16a) with typical bond lengths (1.35 Å for C–N and 1.29 Å for C–O) and angles. The cyanurate anions are stacked antiparallel face-centered along  $[0\ 0\ 1]$  (Figure 16b) to form columns with a hexagonal cross section. These columns are arranged in a hexagonal closest rod packing (Figure 16c).

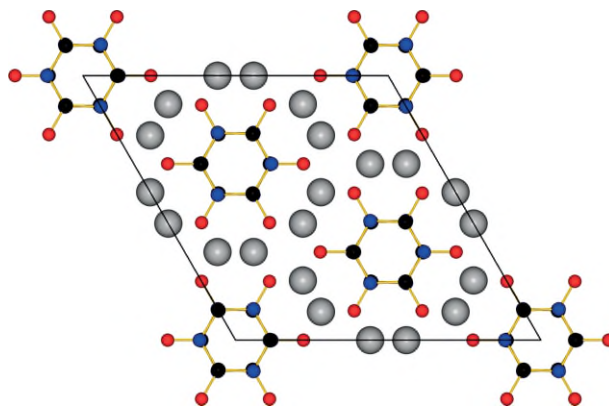


**Figure 15.** The unit cell of  $\text{Na}_3[\text{C}_3\text{N}_3\text{O}_3]$  viewed along  $[100]$ . (Na: grey spheres, C: black spheres, N: blue spheres and O: red spheres, covalent bonds: yellow sticks).

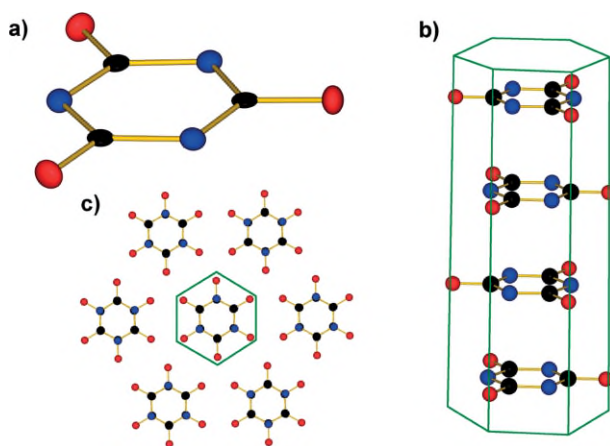


**Figure 16.** Ball-and-stick model of the  $[\text{C}_3\text{N}_3\text{O}_3]^{3-}$  anion of  $\text{Na}_3[\text{C}_3\text{N}_3\text{O}_3]$ ; (a) atoms shown as thermal anisotropic ellipsoids (50%); (b) column resulting from stacked cyanurate anions; (c) rod packing of columns (solid green lines indicate column faces).

$\text{Na}^+$  cations are located on a single crystallographic position in the voids between the columns. They are coordinated by two nitrogen and five carbonyl oxygen atoms forming heavily distorted pentagonal bipyramids (Figure 11b). The interatomic distances between Na and the surrounding atoms correspond on average (2.52 Å) very well with the sum of the ionic radii (2.52 Å). The distorted pentagonal bipyramids are condensed via two common trigonal faces (Figure 17a), forming  $3_1$ - or  $3_2$ -helices along the corresponding screw axis in  $R\bar{3}c$  (Figure 17b). Further condensation via common edges and corners leads to a three-dimensionally condensed framework with hexagonal channels occupied by the mentioned columns of  $[\text{C}_3\text{N}_3\text{O}_3]^{3-}$  anions (Figure 17b).

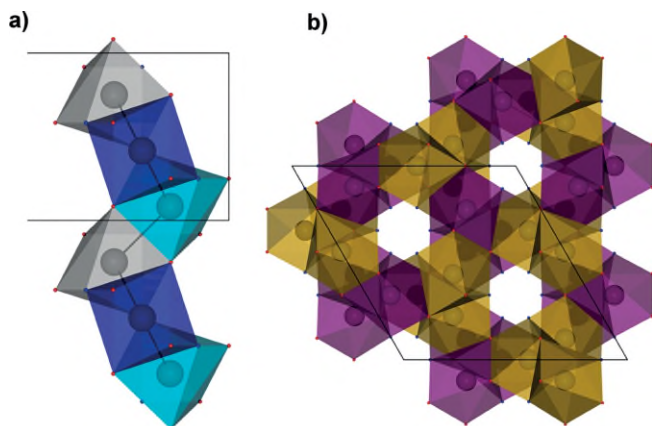


**Figure 17.** Polyhedral representation of the cation environment in  $\text{Na}_3[\text{C}_3\text{N}_3\text{O}_3]$  as pentagonal bipyramids. (a) Condensation via common faces to form a helix (light blue bipyramids on  $c = 1/12$ , dark blue bipyramids on  $c = 5/12$ , grey bipyramids on  $c = 9/12$ ). (b) Further condensation of neighboring helices via common edges and corners ( $3_1$  helices in yellow and  $3_2$  helices in violet).

According to the X-ray powder diffraction pattern (Figure S7, Supporting Information), we were able to synthesize phase pure samples of  $\text{Na}_3[\text{C}_3\text{N}_3\text{O}_3]$ . The FT-IR spectrum is shown in Figure 18, the frequencies of all peaks are tabulated in Table S3 (Supporting Information) and assigned to vibrational modes to the best of the authors' knowledge, as well as compared to frequencies of other tribasic cyanurates and cyanuric acid. The frequencies of all observed bands correspond well with the expected frequencies of the assumed chemical species.<sup>[42,43]</sup> The UV/Vis spectrum (Figure S8, Supporting Information) shows a distinct bandgap absorption edge at about 245 nm, similar to other alkali (iso)cyanurates.<sup>[29]</sup>

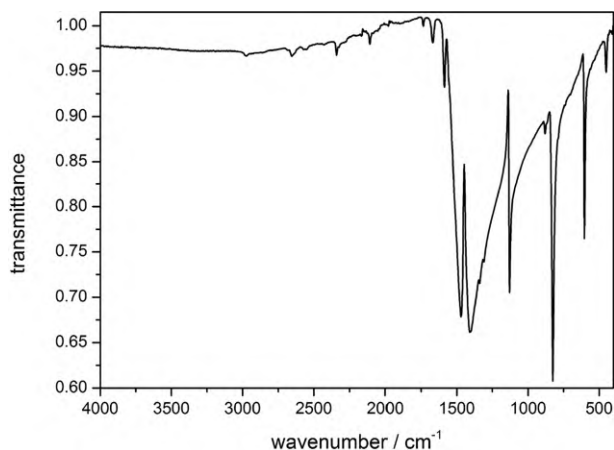


**Figure 18.** FT-IR spectrum of  $\text{Na}_3[\text{C}_3\text{N}_3\text{O}_3]$ .

The thermal decomposition behavior was studied by thermogravimetry and differential scanning calorimetry (Figure 19). The TG curve shows one step of decomposition, which consists of three overlaying substeps. The first substep sets in at about 680 °C and blends into the second substep at about 795 °C with a mass loss of 7.6% up to this point. The second substep ranges from 795 °C to 990 °C and accounts for the largest part of the mass loss of about 73.63%. The third sub-

step starts at about 990 °C and end at about 1090 °C with a mass loss of 8.95%. The DSC curve comprises three major features: a well defined, sharp endothermic signal with an onset at about 650 °C and a maximum at about 705 °C. It directly transitions into a second endothermic feature, which consists of several subsignals that cannot be separated unambiguously and ranges to about 950 °C. The last signal is exothermic and again broad and possibly consisting of several overlapping subsignals. It ranges from about 1000 °C to about 1120 °C and peaks at 1100 °C.

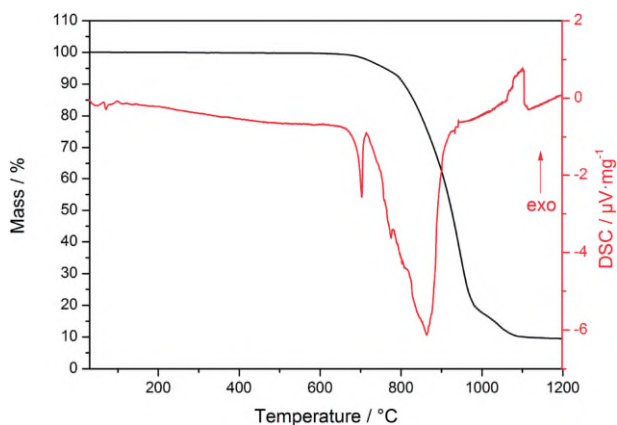


**Figure 19.** TG (black, left ordinate) and DSC curve (red, right ordinate) of  $\text{Na}_3[\text{C}_3\text{N}_3\text{O}_3]$ .

## Discussion

Table 1 gives a short overview of the packing motifs and crystal structures containing only metal cations,  $[\text{H}_{3-x}\text{C}_3\text{N}_3\text{O}_3]$  and  $\text{H}_{2-z}\text{O}$  species known so far, including the members of the  $\text{Na}_x[\text{H}_{3-x}\text{C}_3\text{N}_3\text{O}_3] \cdot y\text{H}_2\text{O}$  series. For merely all monobasic salts, a ribbon motif of hydrogen-bonded  $[\text{H}_2\text{C}_3\text{N}_3\text{O}_3]^-$  is found, with each isocyanurate anion having two N atoms acting as proton donor to two carbonyl groups of two different, adjacent isocyanurate anions and two carbonyl groups acting as acceptors for hydrogen bonds to the same two adjacent isocyanurate anions. This pattern also extends to structures containing additionally fully protonated cyanuric acid or dibasic isocyanurate anions. A notable exception from this pattern is  $\text{Pb}_3\text{O}_2[\text{H}_2\text{C}_3\text{N}_3\text{O}_3]_2$ ,<sup>[22]</sup> which shows a strongly undulated chain.  $\text{Pb}_3\text{O}_2[\text{H}_2\text{C}_3\text{N}_3\text{O}_3]_2$  fits for several reasons rather poorly in this series: it is the only p-block metal salt, its cation coordination environment shows strong sterically active lone-pair effects, and it is the only (iso)cyanurate structure obtained from powder X-ray data. More crystal structures of p-block metal isocyanurates should be elucidated, before  $\text{Pb}_3\text{O}_2[\text{H}_2\text{C}_3\text{N}_3\text{O}_3]_2$  can be unambiguously classified. Regarding the cation substructure, a prevalence of isolated coordination polyhedra and chains of edge-sharing coordination polyhedra is observed, though the trend is much less clear than for the anion substructure.

**Table 1.** Overview of crystal structures and structural motifs of the anion and cation substructure of compounds containing only metal cations,  $[H_{3-x}C_3N_3O_3]$  and  $H_{2-z}O$  species ( $C_3N_3O_3 = \text{cya}$ ).

Chemical formula	Anion topology	Cation topology
<b>Monobasic salts</b>		
Ba $[H_2cya]_2 \cdot 2H_2O$ <sup>[5]</sup>	ribbon	chain
Ba $_3[H_2cya]_2[Hcya]_2 \cdot 4H_2O$ <sup>[29]</sup>	ribbon	layer
Ca $[H_2cya] \cdot 7H_2O$ <sup>[6]</sup>	ribbon	isolated
Co $[H_2cya] \cdot 7H_2O$ <sup>[10,11,14]</sup>	ribbon	isolated
Cs $[H_2cya] \cdot 0.5H_2O$ <sup>[29]</sup>	ribbon	layer
Fe $[H_2cya] \cdot 7H_2O$ <sup>[17]</sup>	ribbon	isolated
K $[H_2cya] \cdot H_2O$ <sup>[8]</sup>	ribbon	layer
K $_3[D_2cya]_3[D_3cya] \cdot 4D_2O$ <sup>[8]</sup>	ribbon	chain
Mn $[H_2cya] \cdot H_2O$ <sup>[11,14]</sup>	ribbon	isolated
Na $[H_2cya] \cdot H_2O$ <sup>[9]</sup>	ribbon	chain
Na $_2Cu[H_2cya]_4 \cdot 6H_2O$ <sup>[12,16]</sup>	ribbon	chain
Ni $[H_2cya] \cdot 7H_2O$ <sup>[11,14]</sup>	ribbon	isolated
Ni $[H_2cya] \cdot 4H_2O$ <sup>[15]</sup>	ribbon	isolated
Pb $_3O_2[H_2cya]_2$ <sup>[22]</sup>	chain	chain
Rb $[H_2cya] \cdot H_2O$ <sup>[29]</sup>	ribbon	chain
Rb $[H_2cya] \cdot H_2O$ <sup>[29]</sup>	ribbon	layer
Rb $_3[H_2cya]_3[H_3cya] \cdot 4H_2O$ <sup>[8]</sup>	ribbon	layer
Sr $[H_2cya]_2 \cdot 4H_2O$ <sup>[29]</sup>	ribbon	isolated
<b>Dibasic salts</b>		
Ca $[Hcya]3.5H_2O$ <sup>[29]</sup>	dimer	layer
Cs $_2[Hcya] \cdot 2H_2O$ <sup>[29]</sup>	chain	framework
K $_2[Hcya]$ <sup>[8]</sup>	chain	framework
Na $_2[Hcya]$	chain	framework
Na $_2[Hcya] \cdot H_2O$	dimer	layer
Sr $[HC_3N_3O_3] \cdot 2H_2O$ <sup>[29]</sup>	chain	layer
Sr $[HC_3N_3O_3] \cdot 3H_2O$ <sup>[29]</sup>	dimer	layer
<b>Tribasic salts</b>		
Ba $_3[cya]_2$ <sup>[20]</sup>	sandwich	framework
Ca $_3[cya]_2$ <sup>[18]</sup>	column	framework
Eu $_3[cya]_2$ <sup>[21]</sup>	column	framework
Na $_3[cya]$	column	framework
Sr $_2[cya]OH$ <sup>[29]</sup>	column	framework
$\alpha$ -Sr $_3[cya]_2$ <sup>[26]</sup>	column	framework
$\beta$ -Sr $_3[cya]_2$ <sup>[21]</sup>	column	framework

For dibasic salts, two structural motifs are found: either the anions form dimers via two hydrogen bonds between the same two isocyanurate anions (involving one N atom as proton donor and the carbonyl group in *ortho* position as acceptor for each of the two isocyanurate species) or the anions adopt a chain motif via two hydrogen bonds between one central and two adjacent isocyanurate anions (involving one N atom as proton donor and the carbonyl group in *para* position as acceptor). So far, apparently structures with a lower content of crystal water tend to form chains, whereas structures with a higher content of water of crystallization tend to form dimers. This can be understood, as the chain motif allows a farther spatial separation of species that are likely to coordinate a metal cation, namely deprotonated N atoms and carbonyl groups not involved in hydrogen bonding, than the dimer motif, so less crystal water is needed to complete the first coordination sphere around the cation. Vice versa, the dimer motif provides more deprotonated N atoms which are too close to coordinating carbonyl groups in order to contribute to the first coordination sphere themselves but still can act as proton acceptors for additional crystal water molecules. This trend does

not seem to depend on the charge of the cation, as it is observed for both  $Na^+$  and  $Sr^{2+}$ , but might still be a size-specific packing effect, as both cations have somewhat similar ionic radii.<sup>[44]</sup> For the cation substructures, layers as well as frameworks of condensed coordination polyhedra are found.

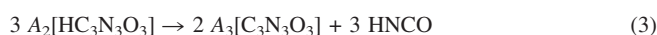
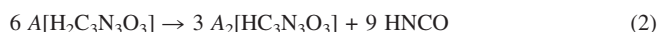
Crystal structures containing tribasic isocyanurate anions typically show parallel stacking of the anions to infinite columns, with varying degree of displacement and rotation. Ba $_3[C_3N_3O_3]_2$  is an exception so far, as only two stapled cyanurate anions form a sandwich configuration, which is surrounded in all directions by cations. This may be attributed to the unusual trigonal prismatic coordination polyhedra around some of the Ba atoms yielding a framework topology that – in stark contrast to all other cation substructures found in this group – contains no hexagonal channels in which columns of  $[C_3N_3O_3]^{3-}$  anions might be situated.

The cation substructure correlates less strictly with the degree of deprotonation, presumably because it is overshadowed by cation size effects on one hand and simple packing effects on the other. Larger cations tend to form condensed coordination polyhedra more readily, as their larger coordination number and longer interatomic distances account for less repulsive Coulomb interaction between them. The ratio of the different constituent chemical species determined by the composition can also force the cation substructure to adopt a different degree of condensation due to simple packing arguments, so that crystal structures with higher metal to crystal water or metal to cyanuric acid ratio, respectively, favor a higher degree of condensation in the cation substructure. This is usually accompanied by an increase in the coordination number of the metal atoms as well as the number of nitrogen atoms in the metal atoms' first coordination sphere. For example, from Na $[H_2C_3N_3O_3] \cdot H_2O$  via Na $_2[HC_3N_3O_3] \cdot H_2O$  and Na $_2[HC_3N_3O_3]$  to Na $_3[C_3N_3O_3]$  the number of coordinating nitrogen atoms (from zero to two) and the coordination number (from six to seven) rise simultaneously with the degree of condensation in the cation substructure, going from chains via layers to a framework motif. This phenomenological approach of classifying metal (iso)cyanurates according to their anion topology can be justified also by considerations of chemical bonding. Though energetically the lattice energy will be dominated by ionic interactions, their isotropic character allows the (iso)cyanurate anions – regarded as rigid bodies hold together by anisotropic covalent bonds – to rotate freely to energetically favorable positions with regard to hydrogen bonds and stacking, leading to characteristic topologies for specific degrees of deprotonation.

As more nitrogen atoms of isocyanuric acid get deprotonated, delocalization of the  $\pi$ -electrons is enhanced and the aromaticity increases, as the keto–enol tautomerism between isocyanurate and cyanurate anions shifts towards the latter. This can be seen in the stepwise shortening of the averaged C–N distances from 1.37 Å in  $H_3C_3N_3O_3$  to 1.35 Å in Na $_3[C_3N_3O_3]$  accompanied by an elongation of the corresponding C–O distances from 1.22 Å, as expected for a typical C=O bond, to 1.29 Å, which is between the typical length of a C=O bond and 1.36 Å, the C–O distance encountered for carboxylate

groups. The IR frequencies associated with ring deformation [ $\delta(\text{NCO})$ ,  $\delta(\text{CNC})$ ,  $\delta(\text{C N})$ ,  $\nu(\text{C-N})$ ,  $\delta(\text{C=O})$ ,  $\pi(\text{CO})$ ] are correspondingly shifted to higher frequencies, whereas the  $\nu(\text{C=O})$  modes are shifted to lower energies mirroring the longer bond length. The increased tendency for especially tribasic salts to stack parallel face-centered might be also attributed to the lesser degree of localization and therefore weaker electrostatic interactions, the latter usually leading to a parallel off-set arrangement, which is encountered more often for isocyanurates with a lower degree of deprotonation.

The thermal decomposition of alkali (iso)cyanurates hydrates is believed<sup>[42]</sup> to follow the following reaction pattern:<sup>[42]</sup>



While this holds reasonably true for  $\text{Na}[\text{H}_2\text{C}_3\text{N}_3\text{O}_3] \cdot \text{H}_2\text{O}$  (measured/theoretical mass loss for the corresponding decomposition steps: (1) 10.7%/9.8%, (2) 39.6%/38.2%, (3) 13.2%/12.7% (4) 35.9%/39.3%), the decomposition of  $\text{Na}_2[\text{HC}_3\text{N}_3\text{O}_3] \cdot \text{H}_2\text{O}$ ,  $\text{Na}_2[\text{HC}_3\text{N}_3\text{O}_3]$ , and  $\text{Na}_3[\text{C}_3\text{N}_3\text{O}_3]$  cannot be understood as easily. In the latter cases, there is significant mass left even at temperatures as high as 1200 °C (pure  $\text{NaNCO}$  should have completely evaporated), similar to what has been found for rubidium and cesium isocyanurates.<sup>[29]</sup> As it is well known for gaseous molecular compounds and cyanate melts,<sup>[45,46]</sup> more complex condensation reactions might happen, which might lead to carbonitridic species of higher thermal stability. The elucidation of possible reaction pathways and identification of the products is still subject of our current research and will be treated in a subsequent study. Heating a  $\text{Na}_3[\text{C}_3\text{N}_3\text{O}_3]$  sample to 650 °C in a tube furnace in a nitrogen stream showed no sign of decomposition, whereas heating it to 700 °C yielded a solidified melt of  $\text{NaOCN}$ . We therefore conclude that the endothermic signal at 705 °C in the DSC curve of  $\text{Na}_3[\text{C}_3\text{N}_3\text{O}_3]$  corresponds to the monomerization of the cyanurate ring accompanied by melting of the resulting sodium cyanate and the second endothermic feature corresponds to evaporation of  $\text{NaOCN}$ . The much lower decomposition point stated by *Seifer*<sup>[42]</sup> (about 430 °C) can be easily explained by one or several unnoticed side phases of less deprotonated cyanurate species: in our experiments, even very small amounts of  $\text{Na}_2[\text{C}_3\text{N}_3\text{O}_3]$  present have significantly decreased the decomposition temperature of the sample, in some cases down to 550 °C. The nature of the exothermic feature at 1100 °C remains unclear, but is probably connected to a more complex condensation reaction to a presumably carbonitridic species, as it coincides with the third substep of weight loss seen in the TG curve of  $\text{Na}_3[\text{C}_3\text{N}_3\text{O}_3]$ .

## Conclusions

In this article we described the syntheses, the crystal structures as determined by single-crystal X-ray diffraction, as well

as the diffractometric, spectroscopic and thermal characterization of  $\text{Na}[\text{H}_2\text{C}_3\text{N}_3\text{O}_3] \cdot \text{H}_2\text{O}$ ,  $\text{Na}_2[\text{HC}_3\text{N}_3\text{O}_3] \cdot \text{H}_2\text{O}$ ,  $\text{Na}_2[\text{HC}_3\text{N}_3\text{O}_3]$ , and  $\text{Na}_3[\text{C}_3\text{N}_3\text{O}_3]$ . The compounds were classified by the topology of their anion substructures, which are formed by hydrogen bonding between and stacking of (iso) cyanurate anions: ribbons for  $\text{Na}[\text{H}_2\text{C}_3\text{N}_3\text{O}_3] \cdot \text{H}_2\text{O}$ , dimers for  $\text{Na}_2[\text{HC}_3\text{N}_3\text{O}_3] \cdot \text{H}_2\text{O}$ , chains for  $\text{Na}_2[\text{HC}_3\text{N}_3\text{O}_3]$ , and columns for  $\text{Na}_3[\text{C}_3\text{N}_3\text{O}_3]$ . These packing motifs are shown to be characteristic for certain degrees of deprotonation and hydration throughout nearly all metal (iso)cyanurate crystal structures determined up to now. We further showed that bond lengths determined by X-ray diffraction and vibrational frequencies determined by IR spectroscopy both show a step wise shift from a typical isocyanurate species towards a bond situation between isocyanurate and cyanurate anion within the keto-enol equilibrium. The thermal decomposition was shown to be much more complicated than believed throughout the literature, and heavily dependant on even very small impurities.

## Experimental Section

**Synthesis:** All compounds were synthesized from  $\text{Na}_2\text{CO}_3 \cdot 10\text{H}_2\text{O}$  (p.a., Merck) respectively  $\text{NaOH}$  (99%, VWR Chemicals), and cyanuric acid (98%, Merck), which were all used without further purification and handled in air. The specific experimental conditions were found empirically, as stoichiometric mixtures of dissolved starting materials tend to form mixtures of several species of cyanuric acid deprotonated to different degrees.  $\text{Na}_3[\text{C}_3\text{N}_3\text{O}_3]$  showed inverse solubility behavior as already mentioned by *Hofmann*.<sup>[38]</sup> While  $\text{Na}_2[\text{HC}_3\text{N}_3\text{O}_3]$  could be obtained from solutions near to the boiling point,  $\text{Na}_2[\text{HC}_3\text{N}_3\text{O}_3] \cdot \text{H}_2\text{O}$  was crystallized at room temperature.

$\text{Na}[\text{H}_2\text{C}_3\text{N}_3\text{O}_3] \cdot \text{H}_2\text{O}$  was synthesized by dissolving  $\text{Na}_2\text{CO}_3 \cdot 10\text{H}_2\text{O}$  (1 mmol, 286.2 mg) and  $\text{H}_3\text{C}_3\text{N}_3\text{O}$  (1 mmol, 129.1 mg) in 10 mL of demineralized water whilst stirring and heating at the boiling point. The solution was concentrated to about 5 mL, causing the product to crystallize. The product was separated from the mother liquor by hot vacuum filtration and the filter cake was dried overnight in air at room temperature. The yield was 27.1%.

$\text{Na}_2[\text{HC}_3\text{N}_3\text{O}_3] \cdot \text{H}_2\text{O}$  was synthesized by dissolving  $\text{NaOH}$  (14.75 mmol, 590 mg) and  $\text{H}_3\text{C}_3\text{N}_3\text{O}$  (5.44 mmol, 702.5 mg) in 20 mL of demineralized water whilst stirring and heating at the boiling point. The solution was concentrated to about 5 mL, during which  $\text{Na}_3[\text{C}_3\text{N}_3\text{O}_3]$  crystallized.  $\text{Na}_3[\text{C}_3\text{N}_3\text{O}_3]$  was removed from the mother liquor by hot vacuum filtration and the product was crystallized by slow evaporation of the obtained filtrate. As this sample contained a small amount of  $\text{Na}_2\text{CO}_3$ , which was probably formed via absorption of  $\text{CO}_2$  from air, it was dispersed in 2 mL of demineralized  $\text{H}_2\text{O}$  via stirring for 30 min, vacuum filtered and the filter cake dried in air at room temperature. The overall yield was 20.4%.

$\text{Na}_2[\text{HC}_3\text{N}_3\text{O}_3]$  was synthesized by dissolving  $\text{NaOH}$  (14.33 mmol, 573.2 mg) and  $\text{H}_3\text{C}_3\text{N}_3\text{O}$  (6.23 mmol, 804.2 mg) in 15 mL of demineralized water whilst stirring and heating at the boiling point. The solution was concentrated to about 5 mL, and at the start of the crystallization of the product the stirring was turned off. The obtained suspension was cooled in an ice bath for 15 min and the product was separated from the mother liquor by cold vacuum filtration. The filter cake was dried overnight in air at room temperature and after removal from the filter for another 15 min at 100 °C in a compartment dryer. The yield was 22.4%.

**Table 2.** Crystal data and structure refinement of Na<sub>2</sub>[HC<sub>3</sub>N<sub>3</sub>O<sub>3</sub>]·H<sub>2</sub>O, Na<sub>2</sub>[HC<sub>3</sub>N<sub>3</sub>O<sub>3</sub>], and Na<sub>3</sub>[C<sub>3</sub>N<sub>3</sub>O<sub>3</sub>].

	Na <sub>2</sub> [HC <sub>3</sub> N <sub>3</sub> O <sub>3</sub> ]·H <sub>2</sub> O	Na <sub>2</sub> [HC <sub>3</sub> N <sub>3</sub> O <sub>3</sub> ]	Na <sub>3</sub> [C <sub>3</sub> N <sub>3</sub> O <sub>3</sub> ]
Formula	Na <sub>2</sub> H <sub>3</sub> C <sub>3</sub> N <sub>3</sub> O <sub>4</sub>	Na <sub>2</sub> HC <sub>3</sub> N <sub>3</sub> O	Na <sub>3</sub> C <sub>3</sub> N <sub>3</sub> O
<i>M<sub>r</sub></i> /g·mol <sup>-1</sup>	191.05	173.04	195.02
Crystal size /mm <sup>3</sup>	0.05 × 0.09 × 0.14	0.01 × 0.02 × 0.24	0.04 × 0.05 × 0.17
Crystal system	triclinic	orthorhombic	trigonal
Space group	<i>P</i> $\bar{1}$	<i>Pnma</i>	<i>R</i> $\bar{3}$
<i>a</i> /Å	3.51660(10)	6.3409(6)	11.7459(3)
<i>b</i> /Å	7.8300(3)	12.2382(13)	11.7459(3)
<i>c</i> /Å	11.3966(4)	6.5919(7)	6.5286(3)
<i>a</i> /°	86.4400(10)	90	90
<i>β</i> /°	85.5350(10)	90	90
<i>β</i> /°	85.0720(10)	90	120
<i>V</i> /Å <sup>3</sup>	311.211(18)	511.54(9)	780.05(5)
<i>Z</i>	2	4	3
<i>D</i> <sub>calcd</sub> /g·cm <sup>-3</sup>	2.039	2.247	2.247
<i>μ</i> (Mo- <i>K</i> <sub>α</sub> ) /cm <sup>-1</sup>	0.294	0.331	0.414
<i>F</i> (000) /e	192	344	576
<i>hkl</i> range	±4, ±9, ±14	±7, ±15, ±8	±14, ±14, ±8
[( <i>sinθ</i> )/ <i>λ</i> ] <sub>max</sub> /Å <sup>-3</sup>	0.62	0.62	0.62
Reflections measured	12230	4192	7985
Reflections unique	1244	516	174
<i>R</i> (int)	0.029	0.039	0.077
Parameter refined	118	56	21
<i>R</i> <sub>1</sub> ( <i>F</i> )/ <i>wR</i> <sub>2</sub> ( <i>F</i> <sup>2</sup> ) (all reflections)	0.030/0.078	0.045/0.079	0.039/0.066
GoF ( <i>F</i> <sup>2</sup> )	1.08	1.06	1.23
<i>Δρ</i> <sub>fin</sub> (max./min.) /e·Å <sup>-3</sup>	0.33/-0.26	0.22/-0.23	0.24/-0.19

Na<sub>3</sub>[C<sub>3</sub>N<sub>3</sub>O<sub>3</sub>] was synthesized by dissolving NaOH (10 mmol, 400 mg) and cyanuric acid (2 mmol, 258.2 mg) in 10 mL of demineralized water whilst stirring and heating at the boiling point. The solution was concentrated to about 4 mL, causing the product to crystallize. The product was separated from the mother liquor by hot vacuum filtration and the filter cake was dried together with the filter paper for 15 min at 80 °C in a compartment dryer. The yield was 27.4%.

**X-ray Structure Determination:** Suited single crystals were selected for single-crystal XRD under a polarized-light microscope. Diffraction data were collected with a Bruker D8 Venture diffractometer using Mo-*K*<sub>α</sub> radiation (*λ* = 0.7093 Å). Absorption correction was performed by the multiscan-method with the program SAINT within the Bruker APEXIII software suite.<sup>[47]</sup> The structures were solved by direct methods and refined by full-matrix least-squares technique with the SHELXTL crystallographic software package.<sup>[48]</sup> The Na, C, N, and O atoms could be directly located, and the hydrogen atoms were either calculated using the AFIX 43 instruction (for some the nitrogen atoms) or assigned from the difference Fourier map and refined with restraints for the hydrogen to donor atom distance using the DFIX instruction (0.99 ± 0.01 Å). Relevant crystallographic data and further details of the structure determinations are summarized in Table 2.

Further details of the crystal structures investigations may be obtained from the Fachinformationszentrum Karlsruhe, 76344 Eggenstein-Leopoldshafen, Germany (Fax: +49-7247-808-666; E-Mail: crysdata@fiz-karlsruhe.de, <http://www.fiz-karlsruhe.de/request> for deposited data.html) on quoting the depository numbers CSD-1871546 (Na<sub>2</sub>[H<sub>2</sub>C<sub>3</sub>N<sub>3</sub>O<sub>3</sub>]·H<sub>2</sub>O), CSD-1871545 (Na<sub>2</sub>[HC<sub>3</sub>N<sub>3</sub>O<sub>3</sub>]·H<sub>2</sub>O), CSD-1871544 (Na<sub>2</sub>[HC<sub>3</sub>N<sub>3</sub>O<sub>3</sub>]) and CSD-1871543 (Na<sub>3</sub>[C<sub>3</sub>N<sub>3</sub>O<sub>3</sub>]).

**X-ray Powder Diffraction:** The X-ray powder diffraction patterns were recorded with a Seifert 3003 TT diffractometer at room temperature in Bragg–Brentano geometry using Cu-*K*<sub>α</sub> radiation, a GE METEOR 1D line detector, and a Ni-filter to suppress *K*<sub>β</sub> radiation (X-ray tube operated at 40 kV and 40 mA, scan range: 5–80°, in-

crement: 0.02°, 40 scans per data point, integration time: 100 s per degree).

**IR spectroscopy:** The infrared spectrum was recorded at room temperature with a Bruker EQUINOX 55 T-R spectrometer using a Platinum ATR device (scan range: 400–4000 cm<sup>-1</sup>, resolution: 4 cm<sup>-1</sup>, 32 scans per sample).

**UV/Vis Spectroscopy:** The UV/Vis spectra were recorded as diffuse reflection spectra at room temperature with a Varian Cary 300 Scan UV/Vis spectrophotometer using an Ulbricht sphere detector and a deuterium lamp / mercury lamp light source (scan range: 200–800 nm, increment 1 nm, scan-rate: 600 nm·min<sup>-1</sup>).

**Thermogravimetry and DSC:** The TG analyses were performed with a NETZSCH STA/TG 409 PC Luxx thermobalance in a nitrogen atmosphere (flow rate: 70 ml·min<sup>-1</sup>) in corundum crucibles (heating rate: 5 K·min<sup>-1</sup>). The DSC analysis were performed with a NETZSCH STA/TG-DSC 409 PC Luxx thermobalance in a nitrogen atmosphere (flow rate: 70 ml·min<sup>-1</sup>) in lidded platinum crucibles with a corundum inlay (heating rate: 5 K·min<sup>-1</sup>).

**Supporting Information** (see footnote on the first page of this article): Further figures illustrating the crystal structures, powder diffraction patterns, UV/Vis spectra, and tables comparing vibrational frequencies.

**Keywords:** Cyanurate; Isocyanurate structure elucidation, sodium, x-ray diffraction, nitrogen heterocycles

## References

- [1] K. Huthmacher, D. Most, in *Ullmann's Encyclopedia of Industrial Chemicals*, Wiley-VCH, **2000**.
- [2] L. E. Erickson, K. H. Lee, *Crit. Rev. Environ. Contam.* **1989**, *19*, 1.

- [3] J. A. Wojtowicz, *J. Swim. Pool Spa. Indust.* **2001**, *4*, 80.
- [4] S. E. Hatfield, Diplomarbeit, Texas A&M University, **2007**.
- [5] C.-Z. Chen, Z.-B. Lin, J.-Q. Shi, X.-Y. Huan, D.-S. Gao, D. Li, H.-Y. Jiang, *Jiegou Huaxue* **1994**, *13*, 468.
- [6] A. N. Chekhlov, *Russ. J. Inorg. Chem.* **2006**, *51*, 799.
- [7] T. F. Syssoeva, M. Z. Branzburg, M. Z. Gurevich, Z. A. Starikova, *J. Struct. Chem.* **1990**, *31*, 602.
- [8] G. S. Nichol, W. Clegg, M. J. Gutmann, D. M. Tooke, *Acta Crystallogr., Sect. B* **2006**, *62*, 798.
- [9] B.-Y. Zhu, J.-D. Fan, W.-T. Yu, D.-L. Cui, H.-P. Jing, *Acta Crystallogr., Sect. E* **2007**, *63*, m1463.
- [10] V. M. Agre, T. F. Sisoeva, V. K. Trunov, M. Z. Gurevich, M. Z. Branzburg, *Koord. Khim.* **1986**, *12*, 122.
- [11] M. Z. Branzburg, T. F. Sisoeva, N. F. Shugal, N. M. Dyatlova, V. M. Agre, M. Z. Gurevich, *Koord. Khim.* **1986**, *12*, 1658.
- [12] R. D. Hart, B. W. Skelton, A. H. White, *Aust. J. Chem.* **1992**, *45*, 1927.
- [13] Z.-B. Lin, C.-Z. Chen, D.-S. Gao, X.-Y. Huang, D. Li, *Chin. J. Struct. Chem.* **1995**, *14*, 61.
- [14] L. R. Falvello, I. Pascual, M. Tomás, *Inorg. Chim. Acta* **1995**, *229*, 135.
- [15] S.-B. Shao, C.-Z. C. X.-Y. Huang, D.-S. G. Z.-B. Lin, D. Li, *Jiegou Huaxue* **1996**, *15*, 246.
- [16] L. R. Falvello, I. Pascual, M. Tomás, E. P. Urriolabeitia, *J. Am. Chem. Soc.* **1997**, *119*, 11894.
- [17] M.-S. Liu, Z.-Y. Zhou, L.-C. Zhu, X.-X. Zhou, Y.-P. Cai, *Acta Crystallogr., Sect. E* **2007**, *63*, m2578.
- [18] M. Kalmutzki, M. Ströbele, F. Wackenhut, A. J. Meixner, H.-J. Meyer, *Angew. Chem. Int. Ed.* **2014**, *53*, 14260.
- [19] M. Kalmutzki, M. Ströbele, H.-J. Meyer, *Dalton Trans.* **2013**, *42*, 12934.
- [20] M. Kalmutzki, M. Ströbele, H. F. Bettinger, H.-J. Meyer, *Eur. J. Inorg. Chem.* **2014**, 2536–2543.
- [21] M. Kalmutzki, M. Ströbele, F. Wackenhut, A. J. Meixner, H.-J. Meyer, *Inorg. Chem.* **2014**, *53*, 12540.
- [22] K. Dolabdjian, M. Ströbele, H.-J. Meyer, *Z. Anorg. Allg. Chem.* **2015**, *641*, 765.
- [23] M. Kalmutzki, M. Ströbele, D. Enseling, T. Jüstel, H.-J. Meyer, *Eur. J. Inorg. Chem.* **2015**, 134–140.
- [24] M. Kalmutzki, X. Wang, A. J. Meixner, H.-J. Meyer, *Cryst. Res. Technol.* **2016**, *8*, 460.
- [25] R. Divya, L. P. Nair, B. Bijini, C. Nair, N. Gopakumar, K. R. Babu, *Phys. B* **2017**, *526*, 37.
- [26] M. Kalmutzki, K. Dolabdjian, N. Wichtner, M. Ströbele, C. Berthold, H.-J. Meyer, *Inorg. Chem.* **2017**, *56*, 3357.
- [27] F. Liang, L. Kang, X. Zhang, M.-H. Lee, Z. Lin, Y. Wu, *Cryst. Growth Des.* **2017**, *17*, 4015.
- [28] M. Xia, M. Zhou, F. Liang, X. Meng, J. Yao, Z. Lin, R. Li, *Inorg. Chem.* **2018**, *57*, 32.
- [29] P. Gross, H. A. Höpfe, *Z. Anorg. Allg. Chem.* **2017**, *643*, 1692.
- [30] S. J. Makowski, E. Calta, M. Lacher, W. Schnick, *Z. Anorg. Allg. Chem.* **2012**, *638*, 88.
- [31] C.-K. Lam, S. C.-K. Hau, C.-W. Yau, T. C. W. Mak, *Cryst. Growth Des.* **2016**, *16*, 759.
- [32] S. Yeom, B. R. Mutlu, A. Aksan, L. P. Wackett, *Appl. Environ. Microbiol.* **2015**, *81*, 6660.
- [33] J. L. Seffernick, L. P. Wackett, *Appl. Environ. Microbiol.* **2016**, *82*, 1638.
- [34] A. K. Bera, K. G. Aukema, M. Elias, L. P. Wackett, *Sci. Rep.* **2017**, *54*, 45277.
- [35] H. C. Hodge, B. J. P. Nad, W. L. Downs, E. A. Maynard, *Toxicol. Appl. Pharmacol.* **1965**, *7*, 667.
- [36] B. G. Hammond, S. J. Barbee, A. G. Wheller, T. Cascieri, *Fundam. Appl. Toxicol.* **1985**, *5*, 655.
- [37] E. Canelli, *Am. J. Public Health* **1974**, *64*, 155.
- [38] A. W. Hofmann, *Ber. Dtsch. Chem. Ges.* **1870**, *3*, 761.
- [39] T. Cascieri, S. Barbee, B. Hammond, T. Inoue, N. Ishida, A. Wheeler, J. Schardein, *Toxicologist* **1983**, *3*, 65.
- [40] A. Wheeler, *Toxicologist* **1985**, *5*, 189.
- [41] T. Cascieri, *Toxicologist* **1985**, *5*, 58.
- [42] G. B. Seifer, *Russ. J. Coord. Chem.* **2002**, *28*, 301.
- [43] R. Newman, R. M. Badger, *J. Am. Chem. Soc.* **1952**, *74*, 3545.
- [44] R. D. Shannon, *Acta Crystallogr., Sect. A* **1976**, *32*, 751.
- [45] E. Irran, B. Jürgens, W. Schnick, *Chem. Eur. J.* **2001**, *7*, 5372.
- [46] A. Sattler, W. Schnick, *Eur. J. Inorg. Chem.* **2009**, 4972–4981.
- [47] Apex3, Bruker AXS Inc., **2015**, Madison, WI, USA.
- [48] G. M. Sheldrick, *Acta Crystallogr., Sect. C* **2015**, *71*, 3.